Journal of Materials and Engineering Structures

Research Paper

Fracture parameters formulation for single edge notched AS4 stitched warp-knit fabric composite plate

Mostefa Lallam [a,b,*], *Said Mamouri* [b], *Abdelkader Djebli* [c]

[a] *Laboratory of Sciences and Water Technical,University of Mustapha Stambouli, Mascara 29000, Algeria*

[b] *University of Tahri Mohamed, Bechar Algeria*

[c] *Laboratory of Quantum Physics of Matter and Mathematical Modeling (LPQ3M), University of Mustapha Stambouli, Mascara 29000, Algeria*

ARTICLE INFO

Article history:

Received : 26 January 2019

Revised : 26 April 2019

Accepted : 9 June 2019

Keywords:

Stress intensity factor

T-stress

Orthotropic materials

Single edge notched plate.

ABSTRACT

The three-dimensional problem of the fracture for the single edge notched tension plate (SENT) of orthotropic material is considered in this paper. The finite element solution is used to evaluate the singular and non-singular terms of the William series, i.e. Stress intensity factor (SIF) and T-stresses namely T_{11}, T_{13} and T_{33}. Based on the obtained numerical results, a fitting procedure is performed in order to propose analytical formulations giving the fracture parameters near the crack tip. The obtained results are in good agreement with the finite elements calculation and other literature results.

1 Introduction

The frequent use of orthotropic materials in industry requires the extension of the concepts of fracture mechanics, which is currently the subject of much research in the world. Most are focused on the first singular term of the Williams series called stress intensity factors (SIF).Irwin establishes the theory of SIF [1] introduced the linear elastic fracture mechanics (LEFM). Later in 1968, Rice defined the J-Integrale independent of the integration path to solve two-dimensional cracking problems in nonlinear elastic materials [2, 3]. In fact, it is well established that J is equivalent to the rate of energy restitution defined by Grifith [4-6]. Thus, J-integral can be used for deduction of SIF [7]. However, the second term of the Williams series, so-

* *Corresponding author. Tel.: +213555009414.*
E-mail address: m.lallam@univ-mascara.dz

e-ISSN: 2170-127X,

RESEARCH REVIEW of Sciences and Technologies

called T-stress provides another parameter to identify the severity of stress and displacement fields near a crack tip [8-10]. In this context, Cotterell worked on the singular term T-stress to predict crack growth paths under Mode I condition [11]. In fact, Cotterell and Rice concluded in [12], that for the crack path is always stable, whereas for T > 0 the propagation becomes unstable. Similar results had been obtained previously in [13, 14], although experimental tests showed the presence of a positive threshold Tth > 0 above which instability of crack propagation occurs [15, 16]. In the same context, the role of T-stress in the brittle fracture for linear elastic materials under mixed-mode loading has aroused an extensive work as like in [17-19], where, Smith et al [20, 21]. had shown that the brittle fracture can be controlled by a combination of singular stresses (characterized by K) or non-singular stress (T-stress). Moreover, in mode II, the T stress is stated to have an influence on the results of the singular stress field [21, 22]. Similarly to isotropic materials, LEFM concepts are used in fracture analysis of orthotropic materials [23-25].

The use of SENT samples in fracture mechanics studies is justified by the fact that surface cracks are common flaws in many structural components [26]. Accurate stress analyses of these surface-cracked components are needed for reliable prediction of their crack-growth rates and fracture strengths.

However, because of the complexities of such problems, exact solutions are not available [27]. The use of approximate fitted analytical equations let engineers to obtain, easily stress-intensity factors for surface cracks under service loading. Moreover, with the development of the numerical tools it has become possible to multiply the simulations with several geometrical parameters. This allowed the researchers to develop simple analytic expressions that calculate fracture parameters that were difficult to compute. The contribution of this work pays in this direction by proposing expressions easy to use and intended for the engineers confronting this kind of design problems.

In this paper, a finite element study is inspired by the published work of Chung-Yi [8] who worked on an orthotropic plate with a central crack. This allowed us to perform the case of single edge cracked orthotropic plate. Thus, the main objective is to propose analytical expressions for a direct calculation of the failure parameters for such case. This is made possible by fitting procedure of the numerical results obtained by the different models.

2 Methodology

In this work the composites with macro through-the-thickness cracks are modeled as linear, orthotropic materials using linear elastic fracture mechanics (LEFM), the Williams series expansion for pure mode I crack-tip fields, including only the singular term and constant term, can be written as [28]:

$$\begin{cases} \sigma_{11} = \dfrac{K_I}{\sqrt{2\pi r}}\cos\dfrac{\theta}{2}\left(1-\sin\dfrac{\theta}{2}\sin\dfrac{3\theta}{2}\right)+T_{11} \\ \sigma_{22} = \dfrac{K_I}{\sqrt{2\pi r}}\cos\dfrac{\theta}{2}\left(1+\sin\dfrac{\theta}{2}\sin\dfrac{3\theta}{2}\right) \\ \sigma_{33} = \dfrac{K_I}{\sqrt{2\pi r}}2\,\upsilon\cos\dfrac{\theta}{2}+T_{33} \\ \sigma_{12} = \dfrac{K_I}{\sqrt{2\pi r}}\sin\dfrac{\theta}{2}\cos\dfrac{\theta}{2}\cos\dfrac{3\theta}{2} \\ \sigma_{13} = T_{13} \\ \sigma_{23} = 0 \end{cases} \quad (1)$$

Where, υ is the Poisson's ratio, r and θ are the polar coordinates in the plane normal to the crack front and the subscripts 1, 2 and 3 designate a local Cartesian system formed by the planes normal, tangential and parallel to the crack front. The magnitude of the singular term K_I is the local mode I stress intensity factor. There are three non-zero components involved in the constant T-stress terms: T_{11}, T_{33} and T_{13}. In practice, T_{11} is usually simply called the T-stress, which represents tensile or compressive stress acting in the crack plane and perpendicular to the crack front, while T_{33} represents the stress acting in the crack plane, and tangent to the crack front. The third T-stress component T_{13} is the shear stress perpendicular to the crack plane. For orthotropic material, these three components are independent of each other for three-dimensional crack front. It can be shown further that T_{11} and T_{13} are related through [8, 29]

$$T_{11}(x_3) = \frac{1}{s'_{11}}\left[I^{(1)}(x_3) - \frac{s_{13}}{s_{33}}\varepsilon_{33}(x_3) \right] \tag{2}$$

$$T_{13}(x_3) = \frac{I^{(2)}(x_3)}{s'_{55}} \tag{3}$$

Where, ε_{33} is the tangent strain component at the crack front, s_{ij} are components of compliance matrix and s'_{ij} are components of reduced compliance matrix for orthotropic material .$I^{(1)}(x_3)$ and $I^{(2)}(x_3)$ are values of the interaction integral [8]. In three-dimensional modeling of crack along a given location x_3, the T_{33} component is also induced by the extension strain $\varepsilon_{33}(x_3)$ along the crack front. Thus, T_{33} can be evaluated as

$$T_{33}(x_3) = \frac{1}{s_{33}}\left[\varepsilon_{33}(x_3) - (s_{13}T_{11} + s_{35}T_{13}) \right] \tag{4}$$

A modified J-integral, namely the equivalent domain integral, is used for a three-dimensional orthotropic cracked solid to evaluate the stress intensity factor along the crack front using the finite element method. Therefore, the local stress intensity factor $k_I(x_3)$ can be calculated as

$$k_I(x_3) = \sqrt{\frac{2J_1(x_3)}{s'_{11}e}} \tag{5}$$

Where, $J_1(x_3)$ represents the value of the equivalent domain integral [8] and e is expression for manipulation of elastic constant eigenvalues.

3 Geometrical Model And Material Properties

The geometry of entire plate considered in this analysis is shown in Figure 1. It has a total length of 2l =2.032 m, a total width of 2w =1.016 m, and a total thickness of 2t =0.0084m.

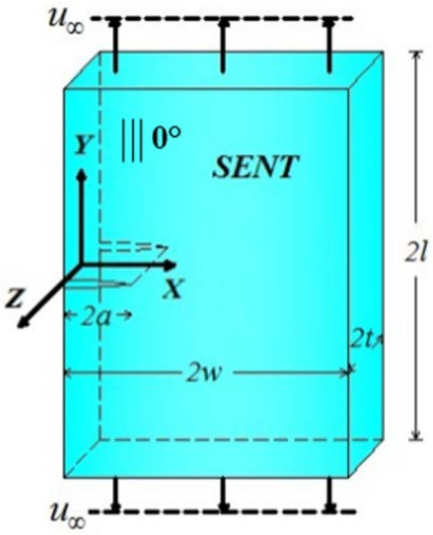

Figure 1: Through-thickness single edge notched cracked plate subjected to a uniform far-field displacement.

The X-axis is parallel to the crack surface and the Y-axis is orthogonal to the crack surface. The Z-axis is normal to the X-Y plane. A uniform displacement u_∞ equivalent to a strain value of 0.1% is prescribed on the far ends at Y =± l.

In these calculations, the composite material considered is AS4 carbon warp-knit fabric [29, 8], designed by the Boeing Company, with six layers of the warpknit fabric (0.0084m). Each layer of fabric with fiber volume content of 59.4% contains AS4 fibers, along the 0° direction (Figure 1) to form the laminate. The resulting materials properties are listed in Table 1.

Table 1: Mechanical properties of the orthotropic plate [29, 8]

E_X (GPa)	E_Y (GPa)	E_Z (GPa)	G_{YZ} (GPa)	G_{XZ} (GPa)	G_{XY} (GPa)	ν_{YZ}	ν_{XZ}	ν_{XY}
35.591	81.172	10.549	4.413	3.930	17.092	0.22	0.29	0.18

Due to heterogeneity in fiber reinforced composites and inhomogeneity in the composite laminates, fracture processes emanating from crack-like flaws are far more complicated than those occurred in metals. In this paper the composites with through-the-thickness cracks are modeled as linear, orthotropic, homogeneous materials using linear elastic fracture mechanics (LEFM) for the purpose of verification and comparison. The effects of microscopic failure mechanisms such as fiber bridging, matrix cracking, and delamination, which accompany fracture, are not taken into account in the modelling. The influence of stitching pattern and knit architecture on the failure initiation of the composites may be of minor importance thus is not considered. This can be argued by a previous studies dealing with this subject [8, 29].

4 Finite elements model

Due to loading and geometry symmetry, just one-quart of a through-thickness SENT specimen is modeled by finite elements. Therefore, symmetric boundary conditions are imposed in the X-symmetry and Z-symmetry places as illustrated in Figure 2. The displacement loading is applied on the surface at Y = l. The finite element model is generated and solved by a general-purpose finite element code ANSYS-12.1 [30]. A typical mesh of the finite element model is shown in Figure 3 and Figure 4. They include coarse 20-node brick-shaped elements called SOLID95 far away from the crack front and refined SOLID95 elements at 20 nodes near the crack front. The elements attached on the crack front are 15-node wedge-shaped elements (SOLID95 element prism option). The overall mesh of L20 model contains 5640 elements and 25183 nodes with 75549 degrees of freedom.

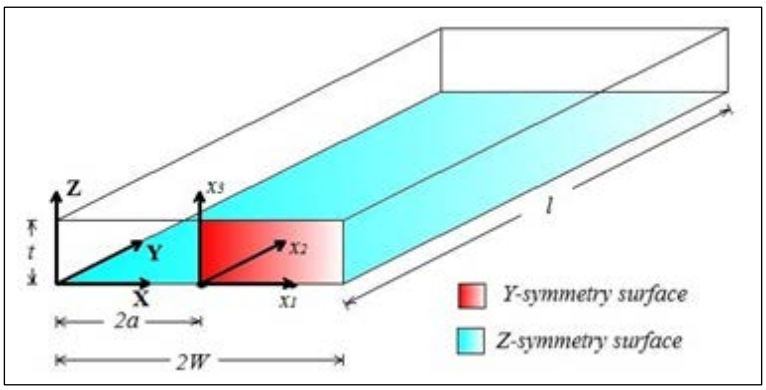

Figure 2: One-quart of the plate to be generated as a geometrical model.

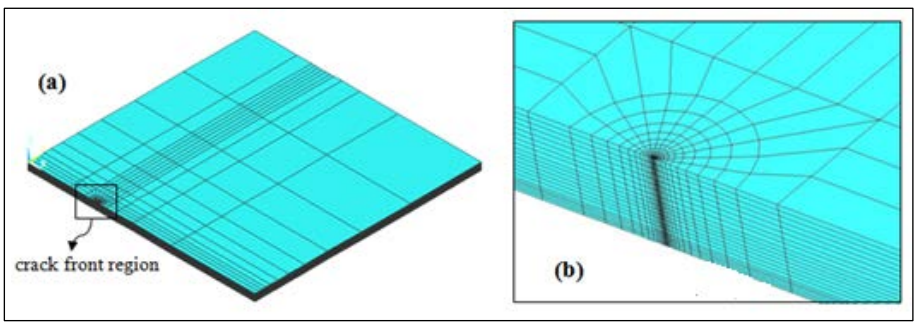

Figure 3: Finite element mesh of a one-quart single edge notched-cracked plate: a) the complete L20 model and b) Zoom of Mesh refinement near crack front region.

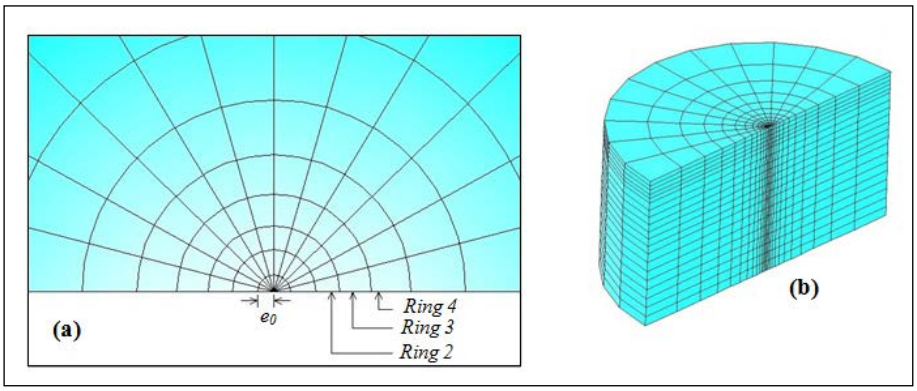

Figure 4 :Mesh detail near the crack front of L20 model a) Detail of radius of the outer surface of Ring near the crack tip and b) Sizes of element layers through of the half thickness t.

4.1 Mesh size effect

A parametric study of the mesh stability is carried out according to the thickness of the SENT models. For this, the half-thickness of the plates is divided respectively into 10,15,20,25 and 30 layers (table 2) to evaluate the effect of the size of elements on the FEM results.

Table 2: Parameters of the different meshes for the study of the mesh stability case of t/w=0.00825

Notation	Number of layers	Number of elements	Number of nodes
L10	10	2988	13043
L15	15	4398	19113
L20	20	5640	25183
L25	25	7050	31253
L30	30	8460	37323

As prospected and in accordance with the literature [31] the mesh size has no effect on the fracture parameters calculated with the energy approach based theory. Effectively, Figures 5, 6, 7 and 8 show clearly the stability of the results for KI, T11, T13 and T33, respectively. Therefore, a choice was made on the L20 model to conduct the rest of the study.

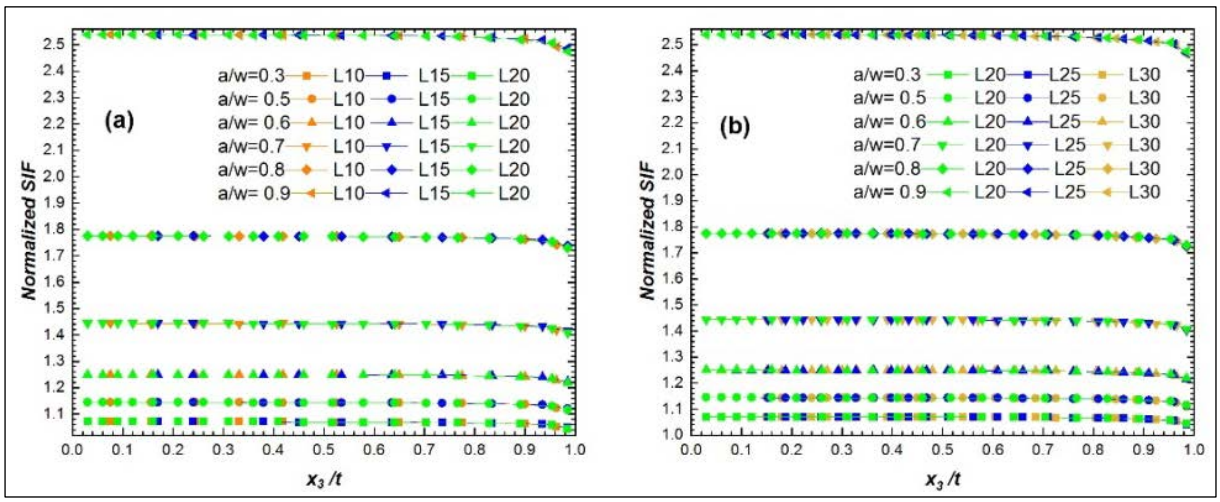

Figure 5: Distribution of the normalized SIF along the crack front for various a/w ratios (case of t/w=0.00825). (a)Finite element models of L10, L15 and L20, (b) Finite element models of L20, L25 and L30

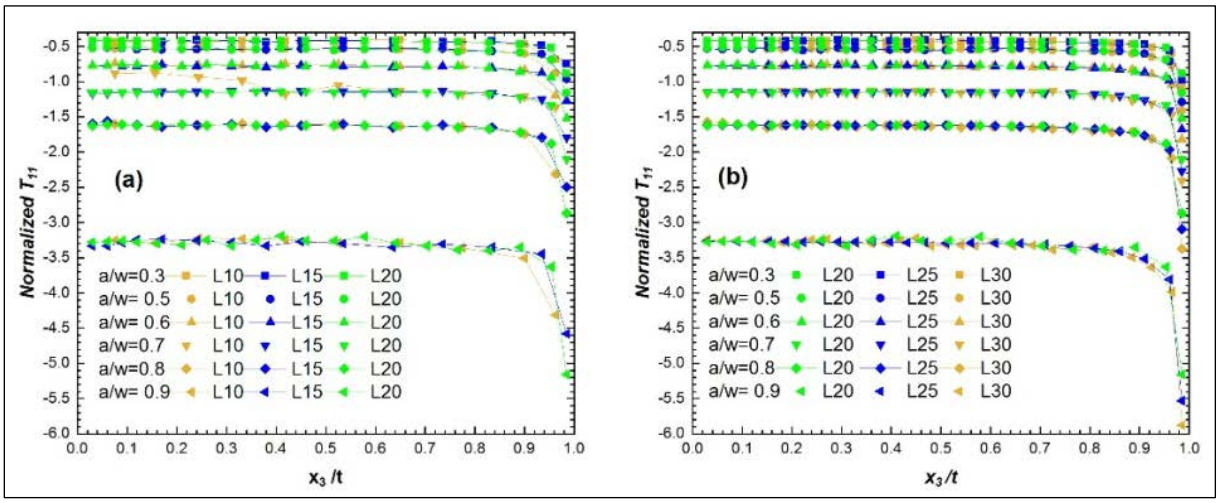

Figure 6: Distribution of the normalized T_{11} along the crack front for various a/w ratios (case of t/w=0.00825). (a)Finite element models of L10, L15 and L20, (b) Finite element models of L20, L25 and L30

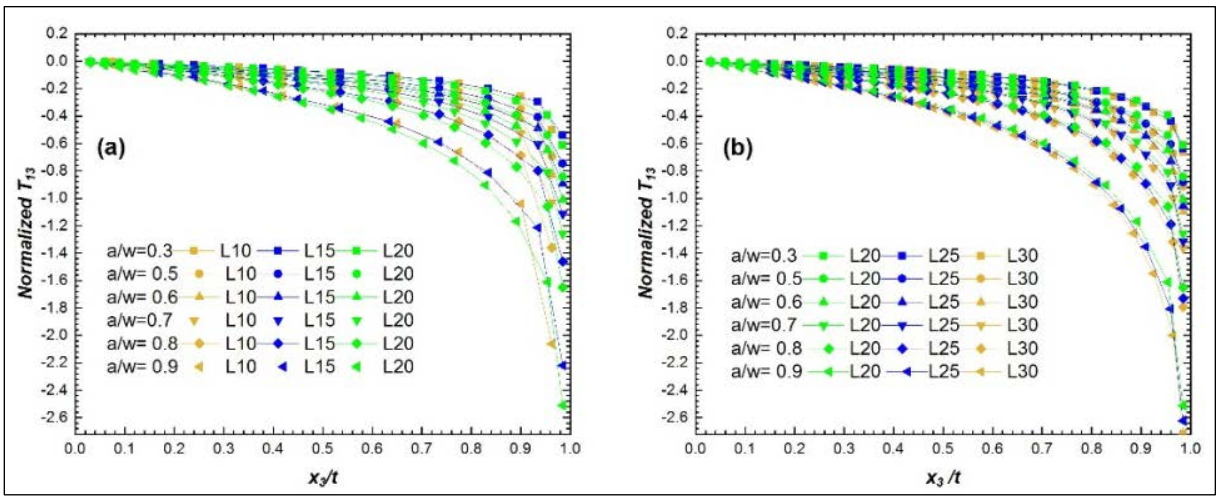

Figure 7: Distribution of the normalized T_{13} along the crack front for various a/w ratios (case of t/w=0.00825). (a)Finite element models of L10, L15 and L20, (b) Ffinite element models of L20, L25 and L30

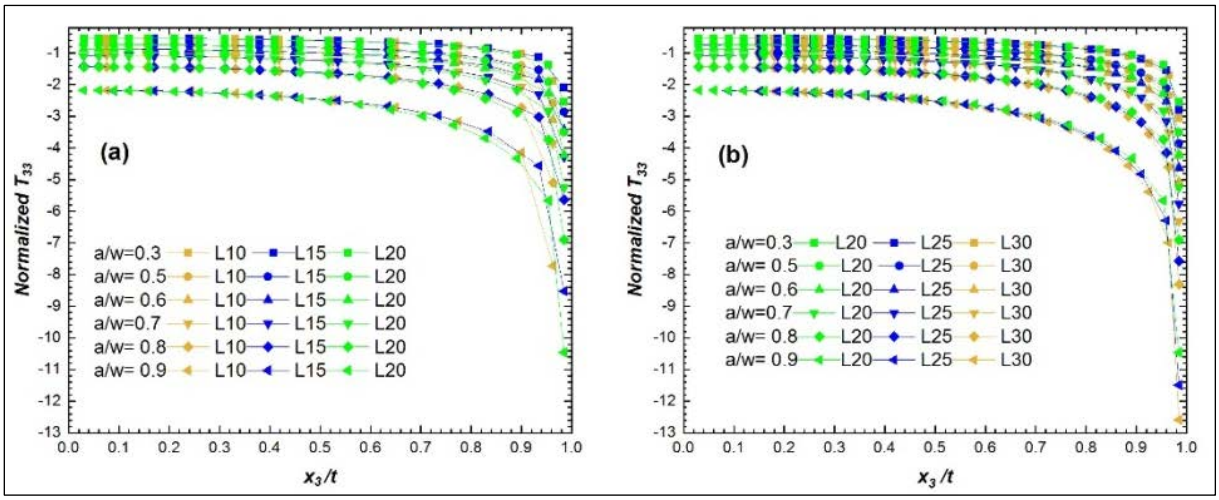

Figure 8: Distribution of the normalized T_{33} along the crack front for various a/w ratios (case of t/w=0.00825). (a)Finite element models of L10, L15 and L20, (b) Finite element models of L20, L25 and L30

5 Results and discussion

5.1 Model Validation

Before addressing the focused analysis, the obtained results are compared to those published by Yuan and Yang [29]. These researchers used methods based on the Betti's reciprocal theorem and the equivalent domain integral (EDI) to extract SIF and T-stress for single edge notched tension (SENT) specimens of stitched warp-knit fabric composites [29, 32]. Table 3 summarizes the comparison between the obtained results. Obviously, present results are in accordance with those given by Yuan and Yang. The largest deviations are 3.96% for stress intensity factor KI and 2.41% for T11 stress.

Table 3: Comparison of fracture parameters for single edge notched tension (SENT) specimens.

a/w	Thickness (mm)	End Disp (mm)	K_I [30] ($MPa\sqrt{m}$)	Actual K_I ($MPa\sqrt{m}$)	Error (%)	T_{11}[29] (MPa)	Actual T_{11} (MPa)	Error (%)
0.25	8.788	1.720	74.062	71.127	3.96	-82.74	-83.36	0.75
0.34	8.585	1.621	85.160	85.172	0.01	-76.53	-78.10	2.05
0.25	8.179	1.306	79.227	78.423	1.01	-124.80	-128.38	2.87
0.33	8.153	1.214	88.127	88.133	0.01	-113.77	-116.039	1.99
0.50	8.103	0.823	75.051	77.845	3.72	-71.71	-69.98	2.41

Next, a comparison of the force versus crack opening displacement (COD) between an experimental test [33] and FEM results for SENT specimens of stitched warp-knit fabric composites is presented in Figure 9. This latter shows a good correlation of the results obtained by the present model.

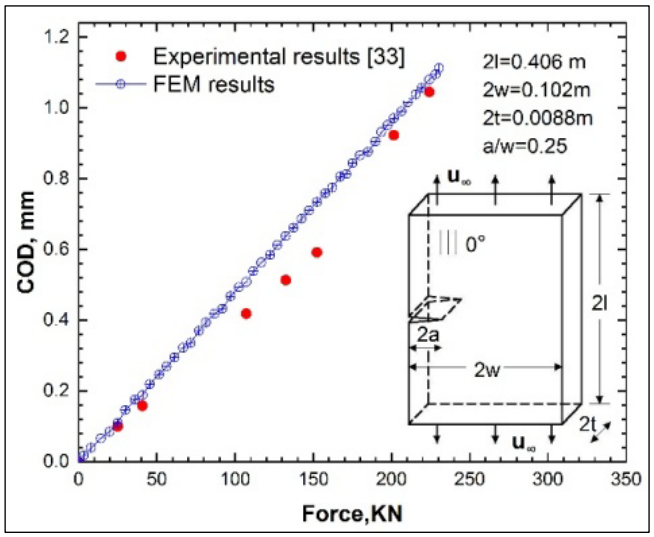

Figure 9: COD versus force for Edge Notch Specimens.

5.2 Finite element results

The normalized stress intensity factor has the form of normalized SIF $=K_I/\sigma_\infty(\pi.a)^{0.5}$, while the normalized T-stresses are defined as normalized $T_{11}=T_{11}/\sigma_\infty$, normalized $T_{13}=T_{13}/\sigma_\infty$ and normalized $T_{33}=T_{33}/\sigma_\infty$. Here σ_∞, is the average stress computed from the total nodal force F resulted from the far-field displacement u_∞, on the plane of Y = l (see Figure 10) divided by the cross-sectional area of the plate. For a cracked plate, $\sigma_\infty=F/(2w.t)$ where 2w is the half width and t is the half thickness. The thickness of the plate is also normalized because the variations of the stress intensity factor and the T-stresses over the thickness are to be investigated. The normalized thickness of an element is defined as normalized $t=x_3/t$. Where, x_3 indicates the coordinate at the center of the element [8]. To determine the distribution of the stress intensity factor and the T-stresses over the thickness of a particular model, these parameters are first calculated from each of the three adjacent rings of

elements very close to the crack front (Rings #2, #3, and #4 as shown in Figure 12.a) by the equivalent domain integral and interaction integral. Then, an average value is carried out over three domains. These average values are calculated as follows:

$$T_{11}(x_3)=\frac{\left(T_{11}(x_3)\right)_{\text{ring }\#2}+\left(T_{11}(x_3)\right)_{\text{ring }\#3}+\left(T_{11}(x_3)\right)_{\text{ring }\#4}}{3} \tag{6}$$

$$T_{13}(x_3)=\frac{\left(T_{13}(x_3)\right)_{\text{ring }\#2}+\left(T_{13}(x_3)\right)_{\text{ring }\#3}+\left(T_{13}(x_3)\right)_{\text{ring }\#4}}{3} \tag{7}$$

$$k_I(x_3)=\frac{\left(k_I(x_3)\right)_{\text{ring }\#2}+\left(k_I(x_3)\right)_{\text{ring }\#3}+\left(k_I(x_3)\right)_{\text{ring }\#4}}{3} \tag{8}$$

It is noted that $T_{33}(x_3)$ depends on the T_{11} and the T_{13} as given by Eq. (4).

Figure 13 presents the normalized SIF curves over half of the thickness for different crack aspect ratios. One can note the symmetry in the distribution of the SIF with respect to x_3=0. It can be mentioned that normalized SIF is relatively stable through the thickness; an exception is noted in the region near the free surface where the latter decreases slightly. This is due to the free surface singularity. The same trend is observed for all analyzed crack lengths (Figure 14). The normalized SIF increases from 1.10 to 2.54 as the a/w ratio increases as shown by Figure 14. The superposition of curve of different thickness indicates that normalized SIF is insensitive to the variation of the plate thickness.

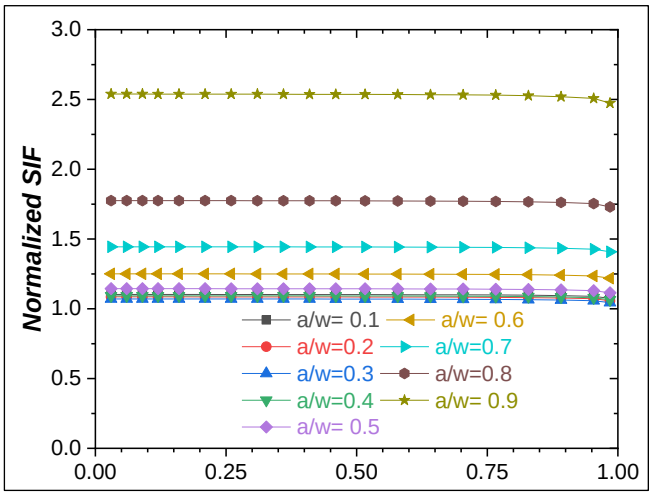

Figure 13: Distribution of the normalized SIF along the crack front for various a/w ratios (case of t/w=0.00825).

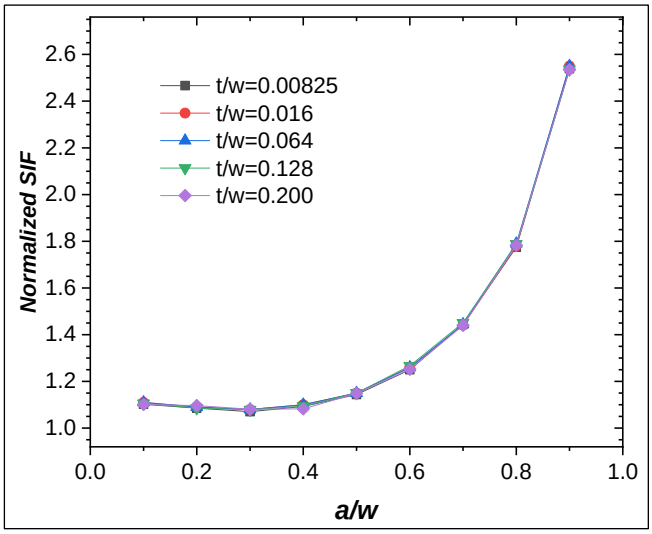

Figure 14: Normalized SIF at the center of crack front for different thicknesses.

In the following, the results relating to the non-singular terms of the William series are presented. For the thinner plate (t/w=0.00825), Figure 15 indicates that the distribution of the normalized T_{11} over a half of the thickness for different crack aspect ratios is symmetric with respect to x_3=0. A relative monotonous distribution of normalized T_{11} is noted over a half of the thickness. An exception is noted in the region near the free surface ($x_3/t \geq 0.85$). This result is consistent with the literature [34-37] which confirms that the crack front intersection with the free surface implies a singularity called weak zone singularity of the corner. Indeed Hartranft and Sih argued in [34] that the classical theory of the singularity of stresses and strains in 2D are not valid for the case of 3D at the free surface because such a field violates the physical characteristics of deformations of the body. This is valid for all plate widths (Figure 15).

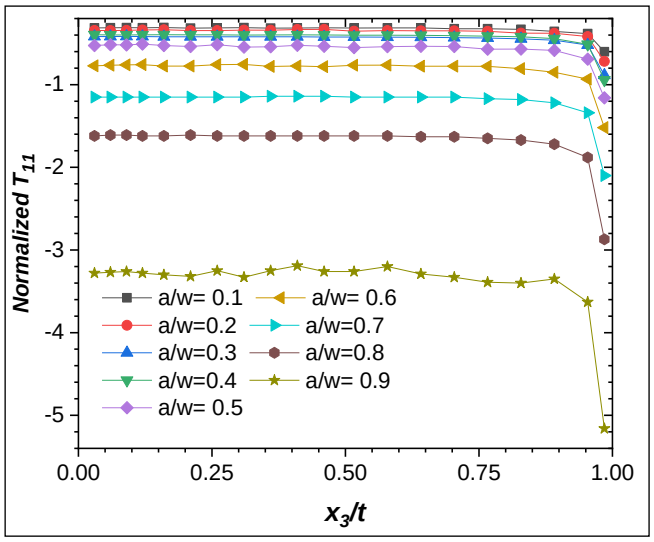

Figure 15: Normalized T_{11} stresses versus the normalized thickness for different lengths (case of t/w=0.00825).

Figure 16 indicates that the value of normalized T_{11} at the center of the thickness decreases gradually from –0.39 to –3.40 as the a/w ratio increases from 0.1 to 0.9. Identical trends are noted for all plate thicknesses indicating the non-dependency of normalized T_{11} term of the plate thickness.

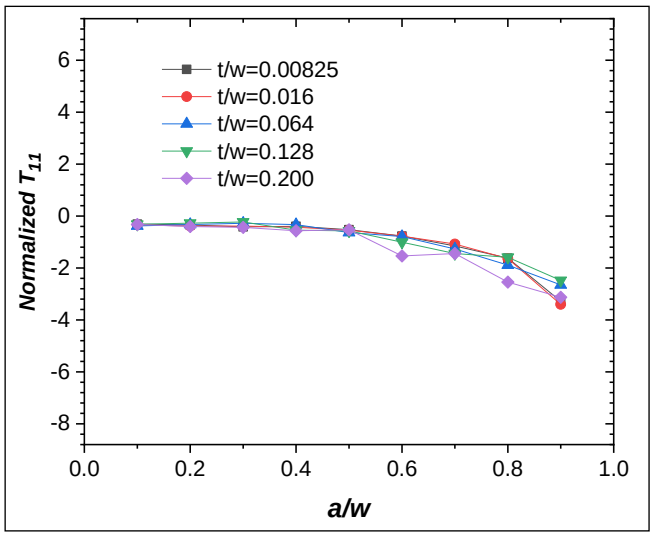

Figure 16: Normalized T_{11} stresses at the center of crack front (x_3/t=0) for different thicknesses.

Figure 17 summarizes the distribution of the normalized T_{13} stresses over the half crack front thickness for the case of the thinner plate (t/w=0.00825) for different a/w ratios. Unlike normalized T_{11}, normalized T_{13} decreases along the crack front thickness. Note that the trend is anti-symmetric with respect to x_3=0 (front center). Instead, the magnitude of the normalized T_{13} stresses decreases gradually from zero at the center of thickness to a much smaller value near the free surface. This latter back to zero to satisfy the unstressed free surface condition.

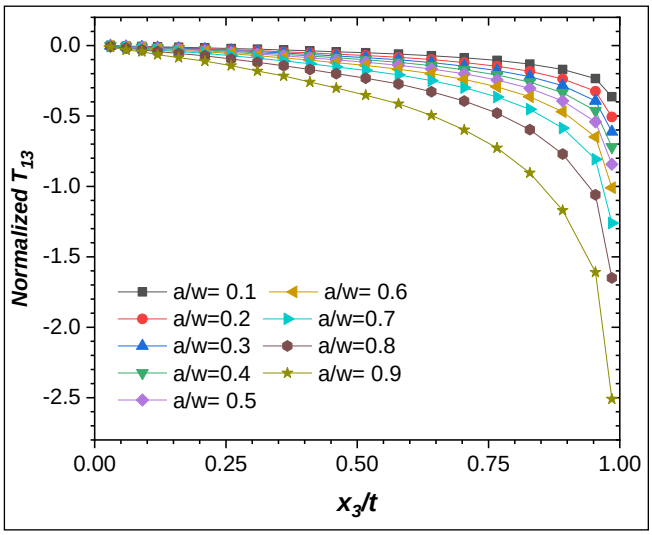

Figure 17: Normalized T13 stresses versus the normalized thickness for different lengths (case of t/w=0.00825).

Figure 18 presents the values of normalized T_{13} at the crack front center versus the crack length ratios for different thickness to width ratios. It can be mentioned that the normalized T_{13} absolute values increase gradually with respect to a/w ratio. Furthermore, it is indicated that T_{13} is sensitive to the change in thickness of the plate.

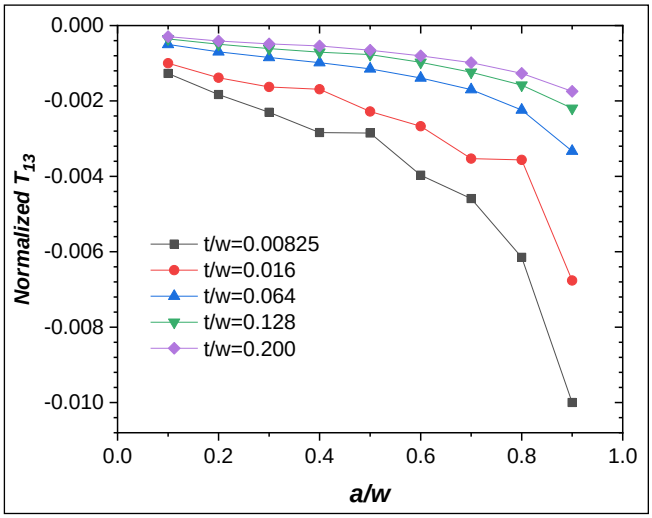

Figure 18: Normalized T13 stresses at the center of crack front (x3/t=0) for different thicknesses.

Figure 19 resumes the obtained results of the third normalized term T_{33}. It can be seen that the trend of normalized T_{33} stress is symmetrical with respect to x_3=0 and it is almost constant when $x_3/t < 0.40$, but decreases behind this position because of boundary effects.

Figure 20 presents the normalized T_{33} at the middle position of the crack front as a function of the crack lengths with respect to different plate thickness. One can see that the T_{33}-stresse increases in absolute value as the crack length increases as well. Figure 20 indicate also that normalized T_{33} is dependent on the plate thickness. This dependency becomes non-significant for large thicknesses.

At this stage, it is possible to fit the various curves presented above. The goal is to formulate analytical expressions including the geometric parameters of crack and plate as variables. These combine different factors of rupture such as SIF and T stresses with the a/w and t/w.

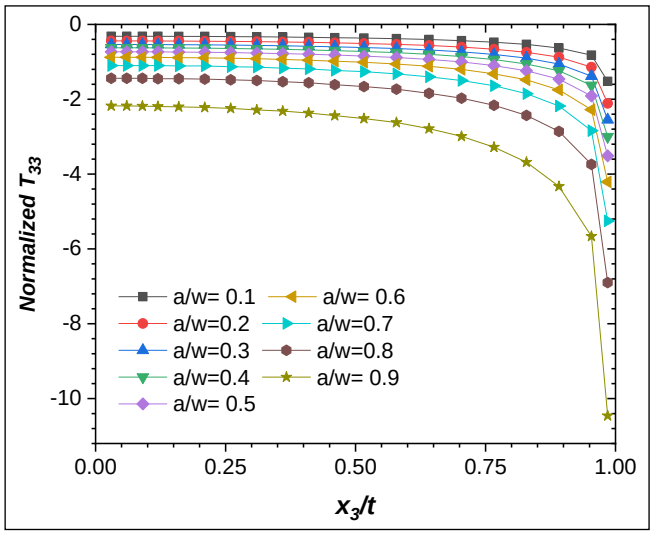

Figure 19: Distribution of the normalized T_{33} stresses through half of the crack front for various a/w ratios (t/w=0.00825).

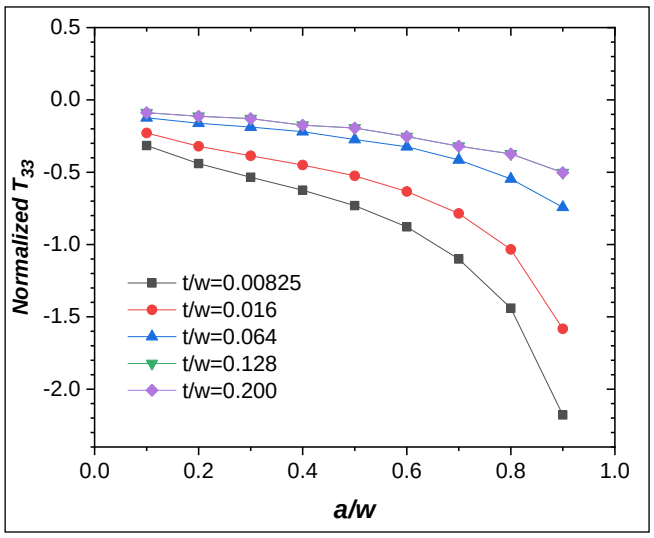

Figure 20: Normalized T_{33} stresses ($x_3/t=0$) for different thicknesses.

5.3 Analytical formulation

Based on the numerical results of the different simulation, analytical expressions have been developed for the convenience of engineering applications. The choice of analytical functions is based on curve fitting trends. More detailed discussion about the fitting method can be developed in [38, 39].The range of applicability of the formulated expressions is $0.1 \leq a/w \leq 0.9$ and $0.00825 \leq t/w \leq 0.200$. As imposed by the trends of the presented curves in Figure 17, The normalized stress intensity factor solutions at $x_3/t=0$ (mid-plan) can be fitted with polynomial equations which are given by cubic form as follows:

$$Normalized\ SIF = A_0 + A_1\left(a/w\right) + A_2\left(a/w\right)^2 + A_3\left(a/w\right)^3 \tag{9}$$

Where A_i are polynomial factors, these factors are obtained by closely adjusting the curves presented in Figure 17.

The coefficients A_i vary slightly in relation to the t/w ratios (Table 4). Thus, by grouping the different ratio of thickness t /w in curves of A_i as a function and making adjustment, it was obtained the following expression:

$$Normalized\ SIF = \left[0.9494\left(\frac{t}{w}\right)^{0.002444}\right] + \left[1.95\left(\frac{t}{w}\right)^{-0.01074}\right].\left(\frac{a}{w}\right) - \left[6.96\left(\frac{t}{w}\right)^{-0.008701}\right]\left(\frac{a}{w}\right)^2 + \left[7.445\left(\frac{t}{w}\right)^{-0.006204}\right]\left(\frac{a}{w}\right)^3 \quad (10)$$

Table 4: Parameters of polynomial equation fitted for normalized stress intensity factors.

t/w	A0	A1	A2	A3
0.00825	0.93906	2.0090	-7.1390	7.5841
0.016	0.93762	2.0991	-7.3766	7.7525
0.064	0.94375	2.0340	-7.2119	7.6452
0.128	0.95096	1.8998	-6.8063	7.3314
0.200	0.94037	2.0351	-7.2117	7.6303

In the same way as for normalized SIF, the normalized T-stresses solutions at $x_3/t=0$ (mid-plan) can be fitted with polynomial equations and written as:

$$Normalized\,T_{11} = B_0 + B_1(a/w) + B_2(a/w)^2 + B_3(a/w)^3 \quad (11)$$

$$Normalized\,T_{13} = C_0 + C_1(a/w) + C_2(a/w)^2 + C_3(a/w)^3 \quad (12)$$

$$Normalized\,T_{33} = D_0 + D_1(a/w) + D_2(a/w)^2 + D_3(a/w)^3 \quad (13)$$

Where, Bi , Ci and Di are polynomial factors which are given in Tables 5, 6 and 7 ,respectively.

Table 5: Parameters of polynomial equations fitted for normalized T_{11}-stresses.

t/w	B0	B1	B2	B3
0.00825	0.1584	-5.6704	17.137	-16.578
0.016	0.19781	-6.6425	19.584	-18.522
0.064	-0.50613	1.358	-1.278	-3.2003
0.128	-0.38433	1.1756	-2.9588	-0.91807
0.200	-0.4641	1.2691	-2.8604	-2.1244

Table 6: Parameters of polynomial equations fitted for normalized T_{13}-stresses.

t/w	C0	C1	C2	C3
0.00825	0.00053135	-0.021083	0.050174	-0.043805
0.016	0.00011168	-0.012882	0.030493	-0.026889
0.064	-1.5264E-05	-0.0057143	0.01297	-0.011827
0.128	-9.62E-05	-0.0031333	0.0066737	-0.0064006
0.200	-0.00011298	-0.0022068	0.0045584	-0.0045596

Table 7: Parameters of polynomial equations fitted for normalized T_{33}-stresses.

t/w	D0	D1	D2	D3
0.00825	0.004208	-3.7738	8.7006	-7.9481
0.016	0.01676	-2.8436	6.6337	-6.005
0.064	0.060286	-0.75488	1.5698	-1.7424
0.128	-0.056606	-0.33875	0.42936	-0.6609
0.200	-0.06459	-0.1529	0.041224	-0.40532

In the same way as for normalized SIF, the analytic expressions of normalized T_{11}, T_{13} and T_{33} are given by writing the different factors B_i, C_i and D_i as adjusted by a power law. As a result, expressions of normalized T_{11}, normalized T_{13} and normalized T_{33} are obtained as follows:

$$Normalized\,T_{11} = -\left[1.98\left(\frac{t}{w}\right)^{0.8102}\right]-\left[0.05514\left(\frac{t}{w}\right)^{-1.005}\right].\left(\frac{a}{w}\right)+\left[0.2471\left(\frac{t}{w}\right)^{-0.9209}\right].\left(\frac{a}{w}\right)^2 - \left[0.9205\left(\frac{t}{w}\right)^{-0.6347}\right].\left(\frac{a}{w}\right)^3 \tag{14}$$

$$Normalized\,T_{13} = \left[6.587\,E-09\left(\frac{t}{w}\right)^{-2.355}\right]-\left[0.0007985\left(\frac{t}{w}\right)^{-0.6805}\right].\left(\frac{a}{w}\right)+\left[0.001643\left(\frac{t}{w}\right)^{-0.7116}\right].\left(\frac{a}{w}\right)^2 - \left[0.001635\left(\frac{t}{w}\right)^{-0.684}\right].\left(\frac{a}{w}\right)^3 \tag{15}$$

$$Normalized\,T_{33} = -\left[3.521\left(\frac{t}{w}\right)^{2.422}\right]-\left[0.1105\left(\frac{t}{w}\right)^{-0.7464}\right].\left(\frac{a}{w}\right)+\left[0.2039\left(\frac{t}{w}\right)^{-0.7947}\right].\left(\frac{a}{w}\right)^2 - \left[0.2496\left(\frac{t}{w}\right)^{-0.7317}\right].\left(\frac{a}{w}\right)^3 \tag{16}$$

5.4 Validation of the proposed analytical expressions

To consolidate the validation of the proposed expressions in this work, it is preceded to a complementary modeling of the orthotropic cracked plate. Different parameters were used compared to the first analysis. Thus, comparison of the obtained by FEM results to those given by the proposed expressions was made. Figures 21.a and 21.b show the example of the normalized K_I calculated by FEM compared to that calculated analytically using equation 10.

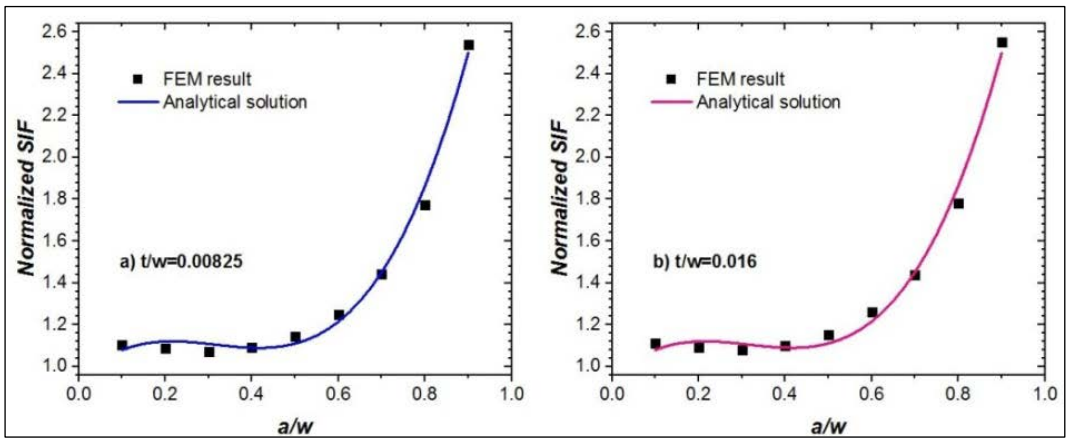

Figure 21: Comparison of FEM results and the proposed expression for normalized stress intensity factor.

It is very clear that the proposed solution fits well with the values obtained numerically. Typical results of T-stresses from finite element analysis and analytical equations for t/w=0.00825 and 0.016 are shown in Figure 22. It can be seen that all the results of the non-singular terms (T-stresses) calculated numerically by FEM are in good correlation with results obtained by the proposed analytical solutions given by equations 14, 15 and 16.

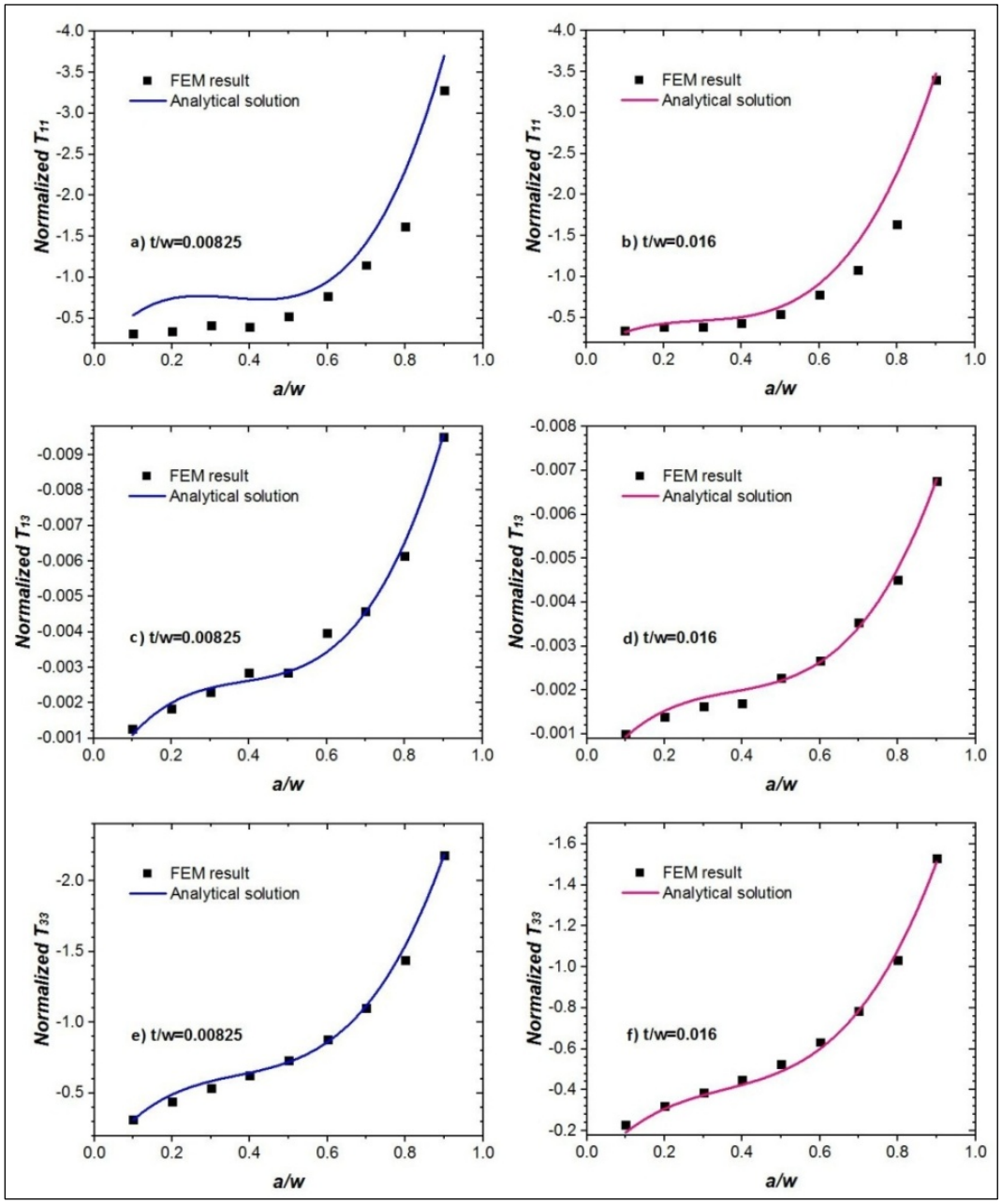

Figure 22: Comparison of FEM results and the proposed expressions for normalized T-stresses: a) Normalized T_{11} for t/w=0.00825, b) Normalized T_{11} for t/w= 0.016,c) Normalized T_{13} for t/w=0.00825, d) Normalized T_{13} for t/w=0.016,e) Normalized T_{33} for t/w=0.00825 and f) Normalized T_{33} for t/w=0.016.

6 Conclusion

A 3D finite element models have been realized to compute the SIF and components of non singular terms T-stress for orthotropic edge cracked plates. A parametric study has been conducted and analytical formulations giving K_I, T_{11}, T_{13} and T_{33} were proposed. The relative crack depth a/w is varied by 0.1, 0.3, 0.5, 0.7 and 0.9. And the relative thickness of the specimen t/w is chosen as 0.00825, 0.016, 0.064, 0.128 and 0.200.

The main conclusions are as follows:

- Stress intensity factor (KI) is independent of the thickness.
- The distribution of SIF adopts the same trend regardless of the thickness in the studied range.
- The same observations are made for the T11.
- The T13 is dependent on the thickness. The latter is anti symmetric.
- The T33 also is dependent on the thickness, but adopts a trend similar to that of KI and T11. In other words, T33 is distributed similarly for the different thicknesses of the orthotropic plate.
- Adequate adjustments can be used to develop simple and easy-to-use expressions for calculating of the fracture parameters. As indicated by the different comparisons, all the results of fracture parameters from analytical expressions are in very good agreement with those performed by the finite element analysis. Thus, for reasons of simplicity, these analytical formulations can be used for the encountered engineering applications dealing with the case of single edge notched cracked orthotropic plates.

As a perspective of this work, it is proposed to realize experimental tests to study the failure behaviour of the used material by using the proposed expressions in this work. These experimental tests allow as to model the crack propagation and to predict the structure lifetime subjected to the same conditions of loading.

REFERENCES

[1]- J.R. Rice, A Path Independent Integral and the Approximate Analysis of Strain Concentration by Notches and Cracks. J. Appl. Mech. 35(2) (1968) 379-386. doi:10.1115/1.3601206.

[2]- D.M. Parks, The virtual crack extension method for nonlinear material behaviour. Comput. Meth. Appl. M. 12(3) (1977) 353-364. doi:10.1016/0045-7825(77)90023-8.

[3]- A.N. Guz, I.A. Guz, A.V. Men'shikov, V.A. Men'shikov, Three-Dimensional Problems in the Dynamic Fracture Mechanics of Materials with Interface Cracks (Review). Int. Appl. Mech. 49(1) (2013) 1-61. doi:10.1007/s10778-013-0551-4.

[4]- A.A. Griffith, The Phenomena of Rupture and Flow in Solids. Philosophical Transactions of the Royal Society of London. Series A, Mathematical, Physical and Engineering Sciences (221)(1921) 582-593. doi:10.1098/rsta.1921.0006.

[5]- D. Gross, T. Seelig, Fracture Mechanics with an Introduction to Micromechanics. 2nd Ed., 2011. doi:10.1007/978-3-642-19240-1

[6]- M. Zakeri, C. Colombo, On the influence of T-Stress on photoelastic analysis under pure mode II loading. Fract. Struct. Integr. 2(3) (2008) 2-10. doi:10.3221/IGF-ESIS.03.01.

[7]- D. Radaj, C.M. Sonsino, W. Fricke, Fatigue assessment of welded joints by local approaches. Second edition, Woodhead Publishing Series, 2006. doi:10.1002/mawe.200690038.

[8]- L. Chung-Yi, Determination of the fracture parameters in a stiffened composite panel. PhD Dissertation, North Carolina State University, Dept. of Mechanical Engineering, NC United States, 2000.

[9]- T. L. Anderson, Fracture mechanics: fundamentals and applications. New York: CRC Press, 1995.

[10]- M.R. Ayatollahi, S.M.J. Razavi, M.R. Moghaddam, F. Berto, Mode I Fracture Analysis of Polymethylmetacrylate Using Modified Energy-Based Models. Phys. Mesomech. 18(4) (2015) 326-336. doi:10.1134/S1029959915040050.

[11]- B. Cotterell, Notes on the paths and stability of cracks. Int. J. Fract. 2(3) (1966) 526-533. doi:10.1007/bf00193691.

[12]- B. Cotterell, J.R. Rice, Slightly curved or kinked cracks. Int. J. Fract. 16(2) (1980) 155-169. doi:10.1007/bf00012619.

[13]- K.G. Kodancha, S.K. Kudari, Variation of stress intensity factor and elastic T-stress along the crack-front in finite thickness plates. Fract. Struct. Integr. 3(8) (2009) 45-51. doi:10.3221/IGF-ESIS.08.04.

[14]- M. Gupta, R.C. Alderliesten, R. Benedictus, A review of T-stress and its effects in fracture mechanics. Eng. Fract. Mech. 134(1) (2015) 218-241. doi:10.1016/j.engfracmech.2014.10.013.

[15]- Y.G. Matvienko, V.S. Pisarev, S.I. Eleonsky, Determination of fracture mechanics parameters on a base of local displacement measurements. Fract. Struct. Integr. 7(25) (2013) 20-26. doi:10.3221/IGF-ESIS.25.04.

[16]- Y. Chao, S. Liu, B. Broviak, B. Brittle fracture: Variation of fracture toughness with constraint and crack curving under mode I condition. Exp. Mech. 41(3) (2001) 232-241. doi:10.1007/BF02323139.

[17]- D.J. Smith, M.R. Ayatollahi, M.J. Pavier, The role of T-stress in brittle fracture for linear elastic materials under

mixed-mode loading. Fatigue Fract. Eng. M. 24(2) (2001) 137-150. doi:10.1046/j.1460-2695.2001.00377.x.

[18]- X. Huang, Y. Liu, X. Huang, Y. Dai, Characteristics and effects of T-stresses in central- cracked unstiffened and stiffened plates under mode I loading, Int. J. Mech. Sci. 133(1) (2017) 704-719. doi:10.1016/j.engfracmech.2017.09.017.

[19]- Y.G. Matvienko, The effect of thickness on out-of-plane constraint in terms of the T-stress. Fract. Struct. Integr. 8(30) (2014) 311-316. doi:10.3221/IGF-ESIS.30.38.

[20]- S. Liu, Y. Chao, Variation of fracture toughness with constraint. Int. J. Fract. 124(3-4) (2003) 113-117. doi:10.1023/b:frac.0000018230.97560.ae.

[21]- M.R. Moghaddam, M.R. Ayatollahi, S.M.J. Razavi, F. Berto, Mode II brittle fracture assessment using an energy based criterion. Phys. Mesomech. 20(2) (2017) 142-148. doi:10.1134/S1029959917020047.

[22]- S. Henkel, E. Liebelt, H. Biermann, S. Ackermann, Crack growth behavior of aluminum alloy 6061 T651 under uniaxial and biaxial planar testing condition. Fract. Struct. Integr. 9(34) (2015) 466-475. doi:10.3221/IGF-ESIS.34.52.

[23]- D. Chakraborty, K. Murthy, D. Chakraborty, Experimental determination of mode I stress intensity factor in orthotropic materials using a single strain gage. Eng. Fract. Mech. 173(2017) 130-145. doi:10.1016/j.engfracmech.2017.01.002.

[24]- C. Bathias, R. Esnault, J. Pellas, Application of fracture mechanics to graphite fiber reinforced composites. Composites 37(12) (1981) 195-200. doi:10.1016/0010-4361(81)90504-8.

[25]- R. Rashetnia, S. Mohammadi, Finite strain fracture analysis using the extended finite element method with new set of enrichment functions. Int. J. Num. Method. Eng. 102(6) (2015) 1316-1351. doi:10.1002/nme.4846.

[26]- J.C. Newman Jr, I.S. Raju. Stress-intensity factor equations for cracks in three-dimensional finite bodies. In : Fract. Mech. : Fourteenth Symposium—Volume I: Theory and Analysis. ASTM International, 1983.

[27]- J.C. Newman Jr, I.S. Raju, An empirical stress-intensity factor equation for the surface crack. Eng. Fract. Mech. 15(1-2) (1981) 185-192. doi:10.1016/0013-7944(81)90116-8

[28]- T. Nakamura, D.M. Parks, Determination of elastic T-stress along three dimensional crack fronts using an interaction integral. Int. J. Solid. Struct. 29(13) (1992) 1597-1611. doi:10.1016/0020-7683(92)90011-h.

[29]- F. Yuan, S. Yang, Fracture behavior of stitched warp-knit fabric composites. Int. J. Fract. 108(1) (2001).73-94. doi:10.1023/A:1007610908503.

[30]- ANSYS Release 12.1, Structural analysis guide, 2009.

[31]- P. Duó, D. Nowell, Use of ABAQUS for stress intensity factors evaluation: comparison with the distributed dislocation method and other numerical approaches. In Proceedings of the 17th UK Abaqus User Group Conference, Coventry, UK, 2003

[32]- F.G. Yuan, Determination of stress coefficient terms in cracked solids for monoclinic materials with plane symmetry at x3=0. NASA Contractor Report, NASA/CR-1998-208729, 1998.

[33]- J.E. Masters, Translaminar fracture toughness of a composite wing skin made of stitched warp-knit fabric. National Aeronautics and Space Administration NASA, 1997.

[34]- R.J. Hartranft, G.C. Sih, Alternating method applied to edge and surface crack problems. In Methods of analysis and solutions of crack problems. In: Methods of analysis and solutions of crack problems. Mechanics of fracture, vol 1. Springer, Ed. Sih G.C., Dordrecht, 1973, pp. 179-238.

[35]- L.P. Pook, Crack profiles and corner point singularities. Fatigue Fract. Engng. Mater. Struct. 23(2000) 141-150. doi:10.1046/j.1460-2695.2000.00249.x.

[36]- V.F. González-Albuixech, E. Giner, J. Fernández-Sáez, A. Fernández-Canteli, Influence of the t33-stress on the 3-D stress state around corner cracks in an elastic plate. Eng. Fract. Mech. 78(2) (2011) 412-427. doi:10.1016/j.engfracmech.2010.11.003.

[37]- M. Heyder, K. Kolk, G. Kuhn, Numerical and experimental investigations of the influence of corner singularities on 3D fatigue crack propagation. Eng. Fract. Mech. 72(13) (2005) 2095-2105. doi:10.1016/j.engfracmech.2005.01.006

[38]- A. Djebli, M. Bendouba, N. Della, A. Aid, A. Benhamena, Finite element modeling and analytical solution of a semi-elliptic crack's J-integral. Recl. Méc. 2(1) (2017) 125-135.

[39]- M. Bendouba, A. Djebli, A. Aid, N. Benseddiq, M. Benguediab, Time-Dependent J-Integral Solution for Semi-elliptical Surface Crack in HDPE. CMC-Comput. Mater. Con. 45(3) (2015) 163-186. doi:10.3970/cmc.2015.045.163.